Stacking-layer-tuned topological phases in $M_2Bi_2Te_5$ (M = Ge, Sn, Pb) films

Yue Li,[1] Yujin Jia,[2,3,4] Bao Zhao,[1,5] Hairui Bao,[1] Hao Huan,[1] Hongming Weng,[2,3,4,*] and Zhongqin Yang[1,6,†]

[1]*State Key Laboratory of Surface Physics and Key Laboratory of Computational Physical Sciences (MOE) and Department of Physics, Fudan University, Shanghai 200433, China*

[2]*Beijing National Laboratory for Condensed Matter Physics, Institute of Physics, Chinese Academy of Sciences, Beijing 100190, China*

[3]*School of Physical Sciences, University of Chinese Academy of Sciences, Beijing 100049, China*

[4]*Songshan Lake Materials Laboratory, Dongguan, Guangdong 523808, China*

[5]*School of Physics Science and Information Technology, Shandong Key Laboratory of Optical Communication Science and Technology, Liaocheng University, Liaocheng 252059, China*

[6]*Shanghai Qi Zhi Institute, Shanghai 200030, China*

(Received 23 December 2022; revised 6 August 2023; accepted 9 August 2023; published 22 August 2023)

With first-principles calculations and theoretical models, we reveal the connection between stacking order, film thickness, and topological behaviors in layered $M_2Bi_2Te_5$ (M = Ge, Sn, Pb) films. We find that single-layer $M_2Bi_2Te_5$ is a topologically trivial indirect band-gap semiconductor. The stacking order drastically tunes the topological property for bilayer $M_2Bi_2Te_5$. In the most stable AB stacking order, bilayer $Pb_2Bi_2Te_5$ is a quantum spin Hall (QSH) insulator with a large band gap of 111.6 meV, accessible for experimental observation. Upon changing the stacking order, one can achieve topological phase transitions between nontrivial and trivial states due to the distinct interlayer coupling. Peculiarly, the multilayer $Pb_2Bi_2Te_5$ film exhibits topological oscillation effect as the film thickness increases from one to six layers. A simplified model Hamiltonian with nearest-neighbor interlayer coupling has been proposed to understand this oscillation. In this paper, we provide a material platform for the realization of controllable topological states, which might stimulate potential applications of topological effects.

DOI: 10.1103/PhysRevB.108.085428

I. INTRODUCTION

Topological insulators (TIs) belong to one type of quantum material which has topology-protected gapless edge states inside the bulk energy gaps [1–9]. Kane and Mele [1,2] proposed the quantum spin Hall (QSH) effect in graphene. Graphene is a seminal and extremely important two-dimensional (2D) material. It has a single-layer hexagonal honeycomb lattice and special Dirac band dispersion. Monolayer graphene can be stacked into bilayer and multilayer structures through van der Waals (vdW) interactions. Double-layer graphene has been explored due to its exotic behaviors [10–15], such as flat bands and superconductivity, coming from the subtle interlayer vdW coupling. Other vdW films or heterostructures, including MoS_2 thin films and bilayer CrI_3, have also been studied [16–24]. Some interesting stacking-related phenomena of electronic states, magnetism, and electronic transport were reported in them. Particularly, in some vdW multilayers, the intriguing topological phases were found to be very sensitive to the thicknesses [25–27] or the stacking patterns [28,29] of the vdW films. The control of film thicknesses and stacking patterns, thus, may become an efficient tuning tactic for the applications of vdW materials in topological electronics. Investigations of topological behaviors of 2D vdW films or heterostructures with respect to the stacking are, however, still very limited.

Compared with ordinary semiconductor crystals and heterostructures, vdW materials have the following advantages: (1) Material synthesis is relatively easy due to the weak vdW interaction between layers [10,17,23]. After high-quality monolayer crystals are grown, multilayer to three-dimensional (3D) crystals can be fabricated by stacking without the problem of lattice mismatch. (2) More degrees of freedom in the vdW crystals or films can be adjusted to tune the electronic states, such as large-scale compression and stretching between the layers and different stacking orders or patterns [14,19]. (3) Based on the recently discovered diverse 2D material systems, different 2D materials can be flexibly combined through vdW interactions. These merits stimulate researchers to design and build various vdW materials with abundant phenomena or effects. Recently, the magnetic vdW materials $MnBi_2Te_4$ and $Mn_2Bi_2Te_5$ have been studied and reported to have unusual topological properties [30–39]. With the advanced molecular beam epitaxy growth technique, high-quality $MnBi_2Te_4$ vdW films have been fabricated experimentally in a layer-by-layer manner by alternate growth of one quintuple layer of Bi_2Te_3 and one bilayer of MnTe [32–36]. Very excitingly, the experimentally rare quantum anomalous Hall effect was observed in atomically thin $MnBi_2Te_4$ [34–36]. In the process of fabricating, if one quintuple layer of Bi_2Te_3 is intercalated by two bilayers of MnTe, $Mn_2Bi_2Te_5$ films can be successfully grown in experiments [39], which were predicted to have intrinsic

*Corresponding author: hmweng@iphy.ac.cn
†Corresponding author: zyang@fudan.edu.cn

topological phases and large dynamical axion field [37,38]. The successful fabrication of the layered $Mn_2Bi_2Te_5$ film [39] and its exotic properties [37,38] has inspired researchers to explore this type of vdW material, just like the role of $MnBi_2Te_4$ films [30–36,40]. Since layered $M_2Bi_2Te_5$ (M = Ge, Sn, Pb) compounds, especially high-quality few-layer $Pb_2Bi_2Te_5$, have been successfully synthesized in experiments [41–44], it is meaningful to explore their electronic states and possible topological behaviors with respect to the layer stacking.

In this paper, we reveal the stacking-layer-tuned topological phases in $M_2Bi_2Te_5$ (M = Ge, Sn, Pb) films through first-principles calculations and an analytic layer-coupling model. Different from $Mn_2Bi_2Te_5$ materials, $M_2Bi_2Te_5$ (M = Ge, Sn, Pb) films have time-reversal symmetry, with QSH effects hopefully obtained. We reveal that monolayer $M_2Bi_2Te_5$ is a topologically trivial indirect band-gap semiconductor. When stacking to a bilayer structure, the stacking order directly affects the topological behavior of bilayer $M_2Bi_2Te_5$. In the most stable stacking order, bilayer $Pb_2Bi_2Te_5$ is found to be a QSH insulator with a large band gap (111.6 meV). After changing the stacking order, a topological phase transition from a topologically nontrivial state to a topologically trivial state occurs. A controllable topological phase transition can also be induced by tuning the interlayer distance. Particularly, we find that multilayer $Pb_2Bi_2Te_5$ exhibits an interesting topological oscillation effect as a function of the layer number, rationalized by a layer-coupling model we built. Not only can this paper help researchers understand well the topological states related to stacking order and film thickness, but we also provide an excellent vdW material platform for the relatively easy experimental realization of the controllable topological phases.

II. MODELS AND METHODS

Here, $M_2Bi_2Te_5$ (M = Ge, Sn, Pb) is a layered ternary tetradymite compound that consists of *ABC* stacking Te1-Bi1-Te2-*M*1-Te3-*M*1′-Te2′-Bi1′-Te1′ nonuple layers (NLs), which has been synthesized in experiments [41–44]. Taking M = Pb as an example, the 1NL geometric structure of $Pb_2Bi_2Te_5$ is shown in Figs. 1(a) and 1(b). Here, 1NL $Pb_2Bi_2Te_5$ has a triangular lattice with the space group of $P\bar{3}m1$ (No. 164). Adjacent atoms in the NL are connected by strong covalent bonds, and the interactions between atoms in the two neighbor NLs are weak vdW interactions. Within 1NL, the stacking order of sequential *A*, *B*, and *C* layers are marked in Fig. 1(b). This structure can be viewed as one quintuple layer of Bi_2Te_3 intercalated by two additional bilayers of *M*Te, like $Mn_2Bi_2Te_5$ [37,38]. Note that all monolayer (namely, 1NL) and multilayer $M_2Bi_2Te_5$ structures simultaneously have inversion symmetry (P) and time-reversal symmetry (T). The space-inversion symmetry owned in the structures guarantees that parity analysis can be adopted to understand the origin of the topological phase transitions.

The geometric optimization and electronic structure calculations of monolayer and multilayer $M_2Bi_2Te_5$ (M = Ge, Sn, Pb) films are performed with the projected augmented-wave [45] formalism based on *ab initio* density functional theory (DFT), as implemented in VASP [46]. The

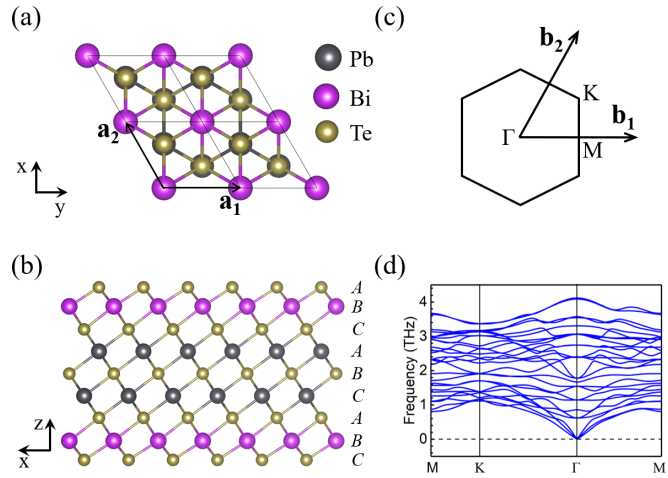

FIG. 1. Geometric structures of monolayer $Pb_2Bi_2Te_5$ from the (a) top and (b) side views. The black arrows (a_1 and a_2) in (a) indicate the reciprocal lattice vectors. (c) The two-dimensional (2D) Brillouin zone. (d) Phonon band dispersion of 1NL $Pb_2Bi_2Te_5$.

Perdew-Burke-Ernzerhof generalized gradient approximation (GGA-PBE) is adopted for the exchange-correlation functional [47]. Interlayer vdW interactions are considered by applying the method of Grimme *et al.* (DFT-D3) [48]. The energy cutoff for the plane-wave expansion is set to be 450 eV, and a vacuum space of 20 Å is considered to exclude the interactions between the two adjacent slabs in the thin film calculations. The convergence criterion for the total energy is set to be 10^{-6} eV. All atoms in the unit cell are allowed to move until the Hellmann-Feynman force on each atom is < 0.01 eV/Å. Here, Γ-centered Monkhorst-Pack k-point meshes of $9 \times 9 \times 1$ are adopted to perform the first Brillouin zone integral. The evolutions of the Wannier charge center (WCC), Z_2, and edge states are performed by constructing the maximally localized Wannier functions [49,50] with the WANNIER90 package [51] and the WANNIERTOOLS code [52]. The phonon band dispersions are calculated based on the PHONOPY code [53,54].

III. RESULTS AND DISCUSSION

A. Electronic states and topological properties of 1NL $M_2Bi_2Te_5$

Since the $Pb_2Bi_2Te_5$ film has the strongest spin-orbit coupling (SOC) interaction and the most obvious topological effect, we will primarily focus on the results of the M = Pb system in $M_2Bi_2Te_5$ (M = Ge, Sn, Pb). The optimized in-plane lattice constants of monolayer and multilayer $Pb_2Bi_2Te_5$ films are shown in Table I. For 1NL $Pb_2Bi_2Te_5$, the optimized lattice constant and the layer thickness are 4.49 and 15.09 Å, respectively. As the NL number increases, the optimized in-plane lattice constant of the thin film becomes close to that of bulk $Pb_2Bi_2Te_5$ (4.51 Å). Since the difference between the in-plane lattice constants of the 3NL film and bulk is very small (∼0.02%), it can be ignored. Thus, the in-plane lattice constants of the films thicker than 3NL are fixed to be that of bulk $Pb_2Bi_2Te_5$ for the subsequent calculations. The calculated phonon band dispersion of 1NL $Pb_2Bi_2Te_5$ shown in Fig. 1(d) has no negative frequencies, indicating the dynamic stability of $Pb_2Bi_2Te_5$.

TABLE I. Summary of the optimized in-plane lattice constants (a), band gaps (E_g), and Z_2 of the 1–6 NL $Pb_2Bi_2Te_5$ thin films. Among them, the in-plane lattice constants of the 3–6NL films are equal to that of bulk $Pb_2Bi_2Te_5$.

Thickness (NL)	a (Å)	E_g (meV)	Z_2
1	4.49	266.5	0
2	4.50	111.6	1
3	4.51	60.2	0
4	4.51	30.4	1
5	4.51	13.2	0
6	4.51	5.7	1

The band structures of 1NL $Pb_2Bi_2Te_5$ obtained from first-principles calculations are illustrated in Fig. 2(a), where the Fermi level (E_F) is set at 0 eV. In the absence of SOC, 1NL $Pb_2Bi_2Te_5$ is a semiconductor with an indirect band gap of 932.3 meV. The conduction band minimum (CBM) is located at the Γ point, while the valence band maximum (VBM) is sited at a point along the K-Γ line. When the SOC is considered, the basic properties of the band dispersion are preserved. The global band gap, however, decreases dramatically to 266.5 meV [Fig. 2(a)], showing very strong SOC interactions existing in the $Pb_2Bi_2Te_5$ monolayer due to the heavy Bi, Pb, and Te atoms in the material. Figure 2(b) shows that no edge states connect the valence and conduction bands. This, together with the WCC evolution in Fig. 2(c), illustrates that 1NL $Pb_2Bi_2Te_5$ is a topologically trivial semiconductor.

The geometric structures and electronic states of $Ge_2Bi_2Te_5$ and $Sn_2Bi_2Te_5$ monolayers are like those of $Pb_2Bi_2Te_5$. The obtained in-plane lattice constants of $Ge_2Bi_2Te_5$ and $Sn_2Bi_2Te_5$ monolayers are 4.33 and 4.44 Å, respectively. They are slightly smaller than that (4.49 Å) of the $Pb_2Bi_2Te_5$ monolayer due to the relatively smaller radiuses of Ge and Sn atoms than that of the Pb atom. The $Ge_2Bi_2Te_5$ and $Sn_2Bi_2Te_5$ monolayers are also both topologically trivial semiconductors with indirect band gaps of 376.6 meV (Fig. S1(a) in the Supplemental Material [55]) and 133.9 meV (Fig. S1(c) in the Supplemental Material [55]), respectively. As shown in Figs. S1(b) and S1(d) in the Supplemental Material [55], there are also no edge states connecting the valence and conduction bands for $Ge_2Bi_2Te_5$ and $Sn_2Bi_2Te_5$ monolayers.

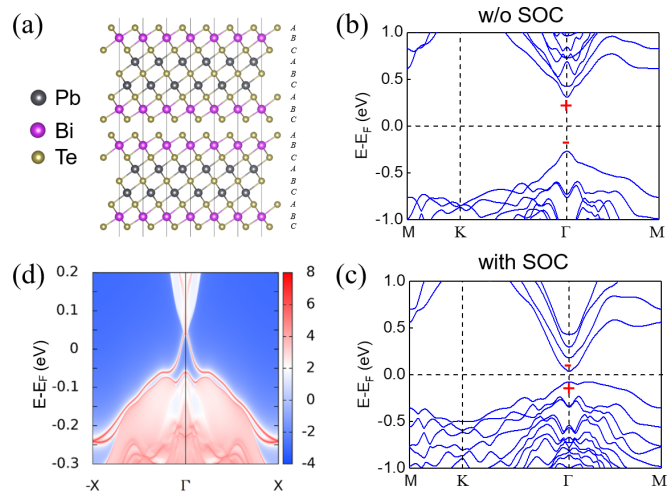

FIG. 3. (a) Side view of the geometric structure of 2NL-1 $Pb_2Bi_2Te_5$. Band structures of 2NL-1 $Pb_2Bi_2Te_5$ (b) without and (c) with spin-orbit coupling (SOC). The red +/− indicates the even/odd parity. (d) Energy and momentum dependence of the local density of states (LDOS) on the (1 1 0) surface of 2NL-1 $Pb_2Bi_2Te_5$.

B. Topological phase transitions of 2NL $M_2Bi_2Te_5$

By stacking two monolayers together, we can get various configurations for bilayer $M_2Bi_2Te_5$ (M = Ge, Sn, Pb) due to the different stacking orders. In the bilayer materials, the two NL building blocks are stacked vertically together through vdW interactions. Taking M = Pb as an example, there are three configurations for 2NL $Pb_2Bi_2Te_5$: 2NL-1 $Pb_2Bi_2Te_5$ [Fig. 3(a)], 2NL-2 $Pb_2Bi_2Te_5$ (Fig. S2(a) in the Supplemental Material [55]), and 2NL-3 $Pb_2Bi_2Te_5$ (Fig. S3(a) in the Supplemental Material [55]), with the stacking orders between the two NLs of *ABC-ABC*, *ABC-CAB*, and *ABC-BCA*, respectively. The optimized in-plane lattice constants, interlayer distances between the two NLs, total energies, and exfoliation energies are shown in Table SI in the Supplemental Material [55]. Comparing with the other two stacking configurations, the first stacking configurations (2NL-1) for all three bilayer materials of $M_2Bi_2Te_5$ (M = Ge, Sn, Pb) have the lowest total energies (Table SI in the Supplemental Material [55]). Thus, they are the most stable structures for the three bilayer materials. The most stable configuration of *ABC-ABC* obtained for

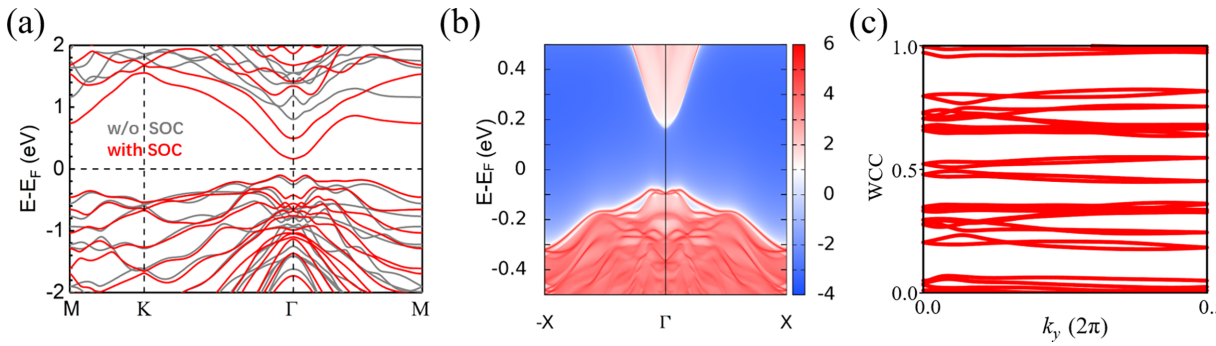

FIG. 2. (a) Band structures of 1NL $Pb_2Bi_2Te_5$ with and without spin-orbit coupling (SOC) considered. (b) Energy and momentum dependence of the local density of states (LDOS) on the (1 1 0) surface of 1NL $Pb_2Bi_2Te_5$. (c) Evolution of the Wannier charge center (WCC).

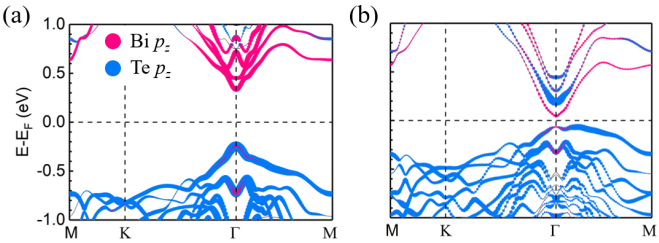

FIG. 4. Orbital-projected band structures of the 2NL-1 $Pb_2Bi_2Te_5$ (a) without and (b) with spin-orbit coupling (SOC). The dot sizes are proportional to the contribution of the corresponding orbitals.

the 2NL $Pb_2Bi_2Te_5$ corresponds to the stacking order of bulk $Pb_2Bi_2Te_5$ [41]. From 2NL-1 to 2NL-3 and 2NL-2, the total energies for $M_2Bi_2Te_5$ (M = Ge, Sn, Pb) increase, ascribed to the increase of the interlayer distances, corresponding to the weaker of the vdW interactions between the two NLs. Additionally, the energy differences between the 2NL-1 and other structures (2NL-2 and 2NL-3) are not large, which are 0.21 and 0.08 eV for 2NL $Pb_2Bi_2Te_5$, respectively. All three stacking orders can, therefore, be expected to be synthesized in experiments. The exfoliation energies of these films are calculated by $E_{exf} = (E_{1NL} - E_{2NL}/2)/A$, where E_{1NL} (E_{2NL}) and A represent the total energy of the unit cell of the 1NL (2NL) film and the in-plane area of the unit cell, respectively. It is reasonable that the most stable stacking order for each type of material has the largest exfoliation energy (Table SI in the Supplemental Material [55]). Their values ($\sim$0.20 J m^{-2}) for the three types of material are all lower than that of graphene exfoliated from graphite (0.37 J m^{-2}) [56], indicating the weaker vdW interactions between the two NLs in the 2NL $M_2Bi_2Te_5$ films.

We now focus on the band structures of the 2NL-1 $Pb_2Bi_2Te_5$ with the most stable stacking order. As displayed in Fig. 3(a), the Bi atoms in the upper NL are right above the Bi atoms in the bottom NL, while each Te atom at the interface in the upper NL is surrounded by three Te atoms in the bottom NL. Considering the coupling between the two NLs, it is expected that 2NL-1 $Pb_2Bi_2Te_5$ will have different behaviors from 1NL $Pb_2Bi_2Te_5$. From Fig. 3(b), one can find that 2NL-1 $Pb_2Bi_2Te_5$ is a semiconductor with a direct band gap of 578.9 meV, smaller than the indirect band gap (932.3 meV) of 1NL $Pb_2Bi_2Te_5$. The VBM of 2NL-1 $Pb_2Bi_2Te_5$ without SOC is mainly contributed by Te p_z orbitals, while the CBM is primarily contributed by Bi p_z orbitals [Fig. 4(a)]. When SOC is considered, the band gap is drastically reduced to 111.6 meV [Fig. 3(c)]. The strong SOC not only decreases the band gap but also causes a band inversion between the VBM and CBM [see Figs. 4(a) and 4(b)]. Moreover, this band inversion accompanies a parity inversion between the VBM and CBM at the Γ point, as marked in Figs. 3(b) and 3(c). Hence, the interlayer vdW coupling and the strong SOC may give rise to a topological phase transition in 2NL-1 $Pb_2Bi_2Te_5$ compared with 1NL $Pb_2Bi_2Te_5$. Because the bands around E_F are primarily composed of p_z orbitals (instead of $p_{x,y}$ orbitals) of Te and Bi atoms, the material properties are very sensitive to the interlayer interactions in multilayer $Pb_2Bi_2Te_5$. Rich topological phase transitions may be induced by tuning the interlayer distance in the film. Note that the electronic correlation effect in $M_2Bi_2Te_5$ systems is not strong, indicated by the large dispersion of the bands around E_F [Figs. 3(b) and 3(c)], although it has been observed in some 2D materials (such as the twisted bilayer graphene [10,11]).

To characterize the topological behavior of 2NL-1 $Pb_2Bi_2Te_5$, we calculate its Z_2 and edge states. The obtained $Z_2 = 1$ and the calculated edge state connecting the conduction and valence bands [Fig. 3(d)] indicate topologically nontrivial behavior with a QSH effect in the 2NL-1 $Pb_2Bi_2Te_5$ film. The topologically nontrivial band gap of 111.6 meV is large enough to observe the QSH effect in experiments at room temperature, which has already been carried out experimentally in several systems, such as HgTe quantum wells [4] and WTe_2 monolayer [57]. The origin of the QSH effect can be ascribed to the vdW coupling of Te atoms between the two NLs and large SOC in the film, which induce the decrease of the band gap and further the band inversion. Therefore, by stacking two 1NL $Pb_2Bi_2Te_5$ films into one bilayer film, the system not only changes from an indirect band-gap semiconductor to a direct band-gap semiconductor, but also there appears a topological phase transition from a trivial state to a nontrivial state.

Whether the topological state appears in bilayer $Pb_2Bi_2Te_5$ is closely related to the stacking orders and coupling strengths of the two NLs. As shown in Table SI in the Supplemental Material [55], the interlayer distances of the 2NL-2 and 2NL-3 $Pb_2Bi_2Te_5$ films are both larger than that of the corresponding 2NL-1 film, giving the weaker interlayer coupling strengths in the 2NL-2 and 2NL-3 stacking orders. Our calculations show that the weaker interlayer vdW interactions do not trigger a topological phase transition in the corresponding systems, as seen from $Z_2 = 0$ in Table SI in the Supplemental Material [55]. At the interface of 2NL-2 $Pb_2Bi_2Te_5$ (Fig. S2(a) in the Supplemental Material [55]), the Te atoms in the upper NL are right above the Te atoms in the bottom NL. This stacking order has the weakest vdW interlayer interactions, resulting in the largest band gap in the material without SOC (Fig. S2(b) in the Supplemental Material [55]). As displayed in Figs. S2(b) and S2(c) in the Supplemental Material [55], the valence band parities of 2NL-2 $Pb_2Bi_2Te_5$ do not change after considering SOC. The calculated $Z_2 = 0$ and no edge states connecting the valence and conduction bands (Fig. S2(d) in the Supplemental Material [55]) also confirm a topologically trivial semiconductor acquired for 2NL-2 $Pb_2Bi_2Te_5$. At the interface of 2NL-3 $Pb_2Bi_2Te_5$ (Fig. S3(a) in the Supplemental Material [55]), the Te atoms in the upper NL are right above the Bi atoms in the bottom NL. The band dispersions of 2NL-3 $Pb_2Bi_2Te_5$ without and with SOC (Figs. S3(b) and S3(c) in the Supplemental Material [55]) are very similar to those of 2NL-1 $Pb_2Bi_2Te_5$ [55]. Due to the larger band gap in 2NL-3 $Pb_2Bi_2Te_5$ than that of the 2NL-1 case, the SOC in the 2NL-3 system cannot cause the band inversion between the VBM and CBM (Figs. S3(b) and S3(c) in the Supplemental Material [55]). No topologically nontrivial edge states appear in the film (Fig. S3(d) in the Supplemental Material [55]). Therefore, like the 2NL-2 case, 2NL-3 $Pb_2Bi_2Te_5$ is also a normal semiconductor. The topological behaviors with respect to the stacking orders for 2NL $Ge_2Bi_2Te_5$ and 2NL $Sn_2Bi_2Te_5$ are like those of 2NL $Pb_2Bi_2Te_5$. Namely, the largest

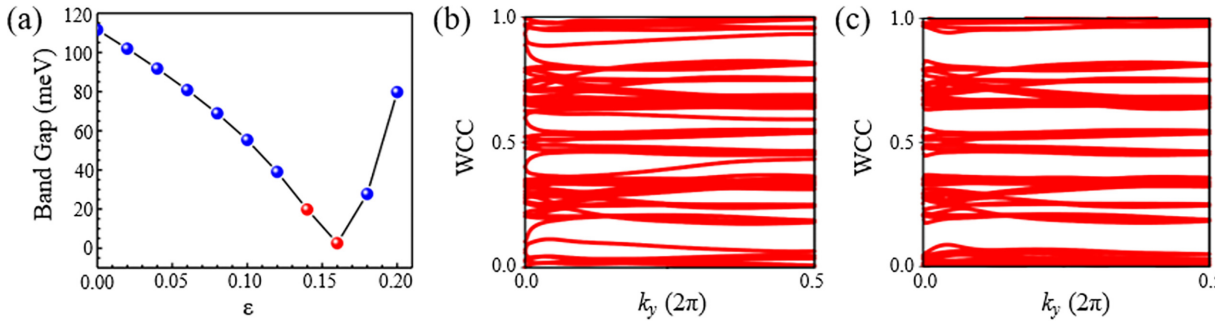

FIG. 5. (a) Band gap at the Γ point around E_F vs the increase of the interlayer distance for 2NL-1 $Pb_2Bi_2Te_5$. (b) and (c) give the Wannier charge center (WCC) when ε are equal to 0.14 and 0.16 [marked in red in (a)], respectively.

interlayer interaction in the 2NL-1 film gives the smallest band gap of the system without SOC. After SOC is turned on, a band inversion between the VBM and CBM occurs in 2NL-1 $M_2Bi_2Te_5$, triggering the topological phase transition. These results clearly demonstrate that stacking orders can vary the topological behaviors of layered materials. The dependence of topological phases on the stacking order was also observed in twisted bilayer systems, such as heterobilayers of massive Dirac materials [28] and twisted bilayer $Bi_2(Te_{1-x}Se_x)_3$ [29]. Hence, varying the stacking order may be an efficient tactic to tune the band topology for vdW materials with small band gaps.

Since the topological states of the bilayer $M_2Bi_2Te_5$ films are sensitive to the coupling strength between the two NLs, a topological phase transition is expected by changing the interlayer distance. For 2NL $Pb_2Bi_2Te_5$, with the gradual increase of the interlayer distance of 2NL-1 $Pb_2Bi_2Te_5$, the band gap of this system first decreases and then increases, as demonstrated in Fig. 5(a), where $\varepsilon = (d - d_0)/d_0$. In the formula, d_0 and d indicate the optimized and tuned interlayer distances, respectively. When the interlayer distance is increased by about $\varepsilon = 0.155$, the band gap is closed. Since the parities of the VBM and CBM of 2NL-1 $Pb_2Bi_2Te_5$ are opposite [Fig. 3(b)], the band inversion occurring in the systems with $\varepsilon > 0.155$ can induce a topological phase transition. Figure 5(b) gives the WCC for the system with $\varepsilon = 0.14$, which together with the calculated $Z_2 = 1$ confirms that the system with $\varepsilon = 0.14$ is still a topologically nontrivial insulator. However, when $\varepsilon \geqslant 0.16$, the obtained $Z_2 = 0$ and the WCC evolution given in Fig. 5(c) indicate the system has transformed into a topologically trivial insulator. Thus, a strong interlayer vdW interaction is crucial to produce the QSH effect in bilayer $M_2Bi_2Te_5$.

Opposite to the 2NL-1 $Pb_2Bi_2Te_5$ film, the 2NL-2 $Pb_2Bi_2Te_5$ and 2NL-3 $Pb_2Bi_2Te_5$ films are both topologically trivial insulators due to the relatively weak interlayer coupling (Table SI in the Supplemental Material [55]). To obtain the QSH effect in the latter films, we increase their interlayer coupling by decreasing the interlayer distance. As illustrated in Fig. S4(a) in the Supplemental Material [55], although the interlayer coupling increases as the interlayer distance decreases and the band inversion occurs (with $\varepsilon \sim -0.10$), no topological phase transition happens in the 2NL-2 $Pb_2Bi_2Te_5$ film owing to the same parities of the VBM and CBM in the system (Fig. S2(c) in the Supplemental Material [55]). Differently, the 2NL-3 $Pb_2Bi_2Te_5$ film has the opposite parities of the VBM and CBM (Fig. S3(c) in the Supplemental Material [55]). When the interlayer distance is reduced with $|\varepsilon| \leqslant 0.05$, $Z_2 = 0$ as well as the WCC in Fig. S4(c) in the Supplemental Material [55] indicates that the system is still a topologically trivial insulator. When the interlayer distance is decreased with $|\varepsilon| \geqslant 0.10$ (Fig. S4(b) in the Supplemental Material [55]), the band inversion occurs, leading to a topological phase transition. The $Z_2 = 1$ as well as the WCC in Fig. S4(d) in the Supplemental Material [55] indicates that the 2NL-3 $Pb_2Bi_2Te_5$ film with $\varepsilon = -0.10$ is a topologically nontrivial insulator. Therefore, tuning the interlayer distance is an effective tactic to induce topological phase transitions in layered $M_2Bi_2Te_5$ films.

C. Topological oscillation effect

Due to the weak vdW interactions between the NLs, the 2D multilayer $M_2Bi_2Te_5$ films can be relatively easily fabricated in experiments by molecular beam epitaxial. We now explore the electronic properties of the multilayer $Pb_2Bi_2Te_5$ films with the most stable stacking order of *ABC-ABC* between the two neighbor NLs. We find that there is an interesting topological phase oscillation as the structure evolves from a monolayer to multilayers. As shown in Fig. 6, the band structures of the multilayer $Pb_2Bi_2Te_5$ films are very similar to each other after the film thickness is larger than 2NL. They are all direct band-gap semiconductors with the VBM and CBM both located at the Γ point. Due to the quantum confinement effect, the energy gap of the $Pb_2Bi_2Te_5$ film with SOC gradually decreases with the increase of the film thickness (Table I).

By calculating the topological invariants of Z_2 and the edge states (Fig. 7) of the 1–6NL $Pb_2Bi_2Te_5$ films, we find that, as the film thickness increases, the QSH state first appears in the 2NL system with the largest (111.6 meV) topologically nontrivial band gap. When the film thickness increases, the topological phase oscillation effect occurs as the film thickness changes by 1NL. As illustrated in Fig. 7, there are 0, 2, and 4 edge states connecting conduction and valence bands in 1NL, 3NL, and 5NL $Pb_2Bi_2Te_5$, respectively. Because the number of edge states is even, an energy gap can appear in the edge states under external disturbances. Therefore, these edge states are not topologically robust. Dissimilarly, there are 1, 3, and 5 edge states connecting conduction and valence bands in 2NL, 4NL, and 6NL $Pb_2Bi_2Te_5$, respectively. Because the number of edge states is odd, if the energy gap of the system is not closed by the external disturbance, there will always be edge states in the energy gap. The E_F can always intersect

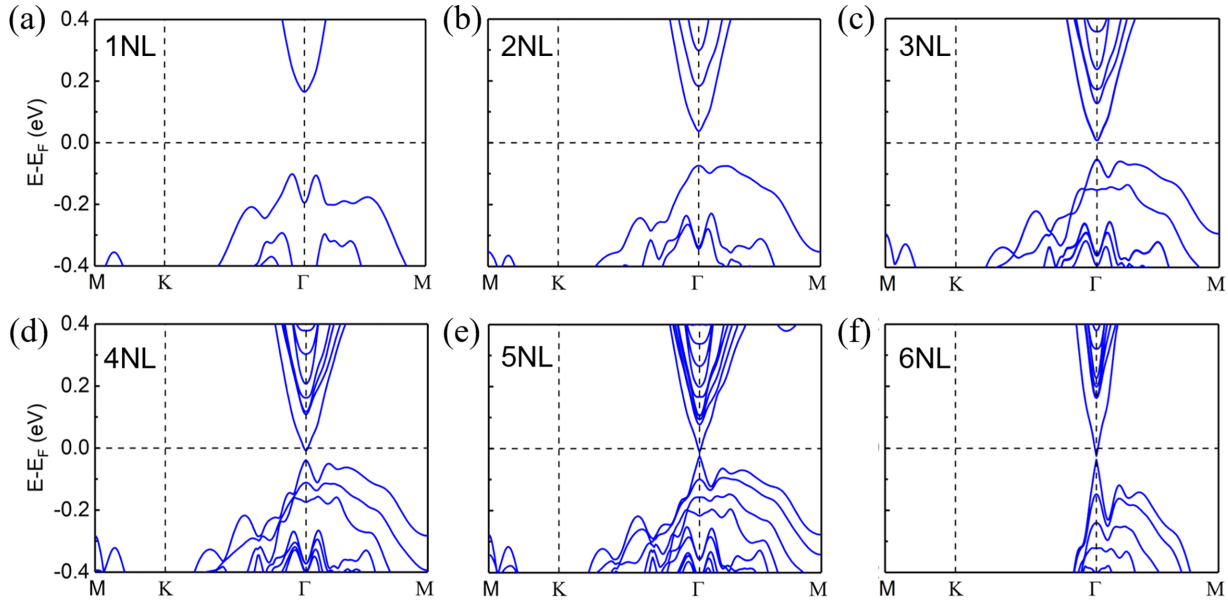

FIG. 6. (a)–(f) Band structures of 1–6 NL $Pb_2Bi_2Te_5$ films with spin-orbit coupling (SOC), respectively.

the edge states by an odd number of times, indicating 2NL, 4NL, and 6NL $Pb_2Bi_2Te_5$ are topologically nontrivial. These edge states are robust and protected by the topology of the film materials. Thus, the topological behaviors of $Pb_2Bi_2Te_5$ films have an interesting oscillation effect with respect to the film thickness. The results of the energy gaps and the change of Z_2 values of the 1–6NL $Pb_2Bi_2Te_5$ films as functions of the film thickness are summarized in Fig. 8. Topological oscillation effects with different characteristics have also been found in other vdW multilayers. For example, the topological oscillation period in Bi_2Se_3 films is 3 layers instead of 1 layer [25]. If the band gaps in $Ge_2Bi_2Te_5$ and $Sn_2Bi_2Te_5$ (Table SI in the Supplemental Material [55]) are large enough, we expect that the oscillation of the topological phases with respect to the thickness may also occur.

As introduced in Ref. [27], bulk $Pb_2Bi_2Te_5$ is a strong 3D TI. Thus, the CBM and VBM in 6NL $Pb_2Bi_2Te_5$ [Fig. 6(f)] can be regarded as the topological surface states of the 3D bulk $Pb_2Bi_2Te_5$ TI. The small band gap (5.7 meV) existing in the 6NL $Pb_2Bi_2Te_5$ film will disappear with the increase

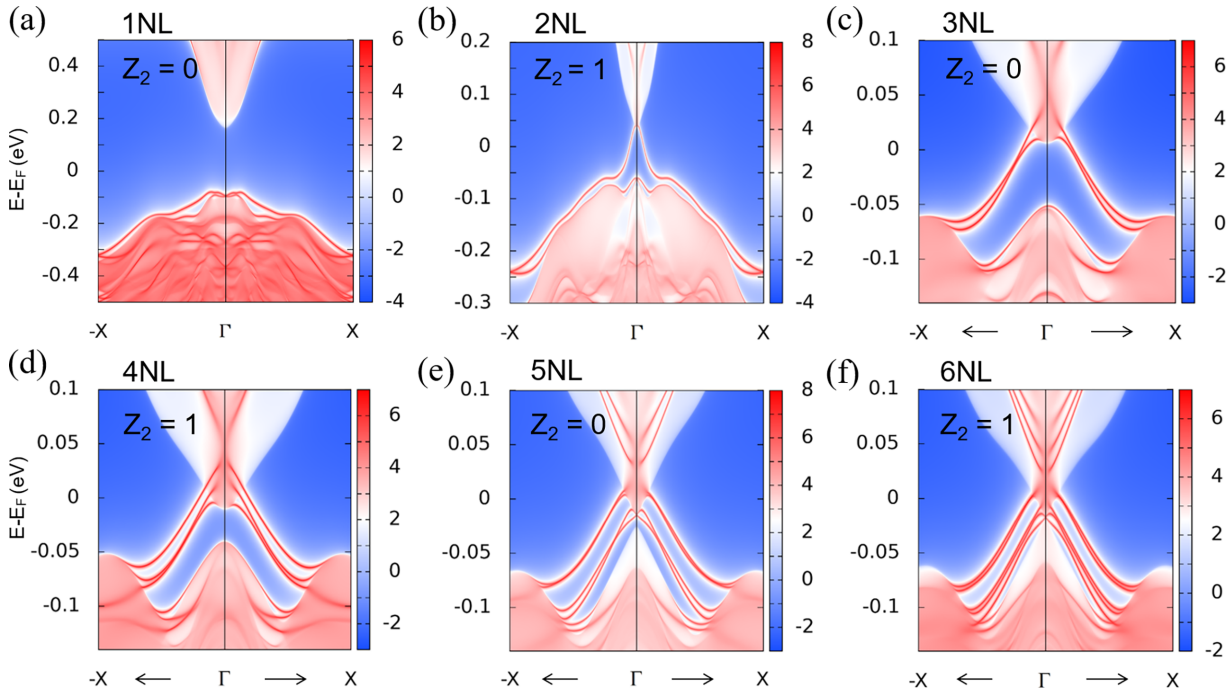

FIG. 7. (a)–(f) Energy and momentum dependence of the local density of states (LDOS) on the (1 1 0) surface of 1–6 NL $Pb_2Bi_2Te_5$ films, respectively.

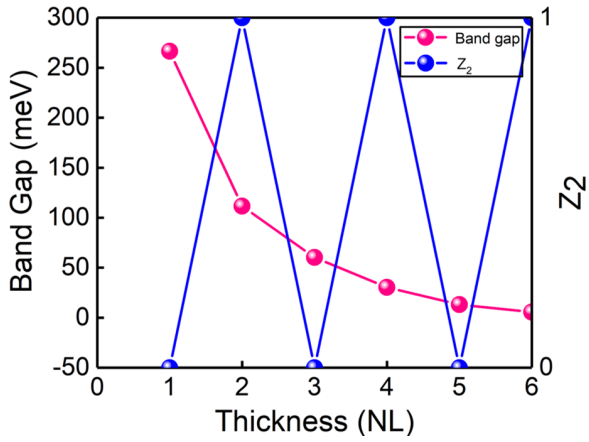

FIG. 8. Band gaps and Z_2 values vs film thicknesses for the $Pb_2Bi_2Te_5$ film. The pink curve indicates band gaps, and the blue curve indicates Z_2 values.

of the film thickness. As far as the relationship between the oscillating 2D topological invariant and the bulk invariant, it is not a simple question. For example, the topological oscillation effects with respect to the film thickness were also found in Bi_2Se_3 and Bi_2Te_3 systems [25], whose bulks are both 3D TIs. The characteristics of the topological oscillations for the two films are, however, various. The former has an oscillation period of 3 layers, while the latter has a period of 1 layer (the same as that of the $Pb_2Bi_2Te_5$ film studied here). There does not seem to be a straightforward rule for the relationship between the 2D and 3D topological behaviors.

D. Theoretical model for the topological oscillation effect

To understand the topological phase oscillation as the layer stacking changes, a conduction-valence band analytic model Hamiltonian has been constructed. Since the topological phase transition all happens with the band inversion at Γ, we only discuss the Hamiltonian and the bands at Γ. We start with the Hamiltonian of single-layer 1NL, $H_1 = \begin{pmatrix} \epsilon_c & 0 \\ 0 & \epsilon_v \end{pmatrix}$, where $\epsilon_c > 0$ and $\epsilon_v < 0$ are conduction and valence band energies, respectively. For simplicity, the coupling of the conduction and valence bands is neglected, and their eigenwave functions are used as the basis sets to build the Hamiltonian of multilayer cases. Only the coupling between the nearest vdW layers is considered here. The parities of the conduction and valence band wave functions are assumed to be even (denoted as +), consistent with the trivial band structure of 1NL.

TABLE II. Solutions of the 2NL system, by diagonalizing its Hamiltonian.

Order	Band energy	Wave function	Parity
C1	$\epsilon_c + t_c$	1, 0, 1, 0	+
C2	$\epsilon_c - t_c$	−1, 0, 1, 0	−
V1	$\epsilon_v + t_v$	0, 1, 0, 1	+
V2	$\epsilon_v - t_v$	0, −1, 0, 1	−

For the 2NL system, the Hamiltonian can be written as

$$H_2 = \begin{pmatrix} \epsilon_c & 0 & t_c & 0 \\ 0 & \epsilon_v & 0 & t_v \\ t_c & 0 & \epsilon_c & 0 \\ 0 & t_v & 0 & \epsilon_v \end{pmatrix},$$

where $t_c > 0$ and $t_v > 0$ are the nearest-neighbor coupling strength for the conduction and valence bands, respectively. Therefore, the Hamiltonians of the 3NL, 4NL, 5NL, and 6NL systems are 6×6, 8×8, 10×10, and 12×12 matrices with similar forms, respectively.

In Table II, the solutions to the 2NL Hamiltonian are shown. Due to the interlayer coupling, the conduction band splits into two bands: C1 and C2. The case is similar for the valence band. In Fig. 9, when $\epsilon_v + t_v > \epsilon_c - t_c$, V1 with even parity + goes up in energy and finally lies above E_F, while C2 with odd parity − moves down in energy and lies below E_F. This band inversion leads to the nontrivial topology of $Z_2 = 1$ for the 2NL system. If there is no such band inversion, it is adiabatically equivalent to simple stacking of two single layers of $Z_2 = 0$, which is obviously topologically trivial.

For the 3NL system, the model Hamiltonian gives out a similar solution, listed in Table III. In Fig. 10, from the condition that satisfies 2NL being topologically nontrivial, there must have $\epsilon_c - \sqrt{2}t_c < \epsilon_c - t_c < \epsilon_v + t_v < \epsilon_v + \sqrt{2}t_v$. Therefore, the C3 energy level moves down and inverts with V1

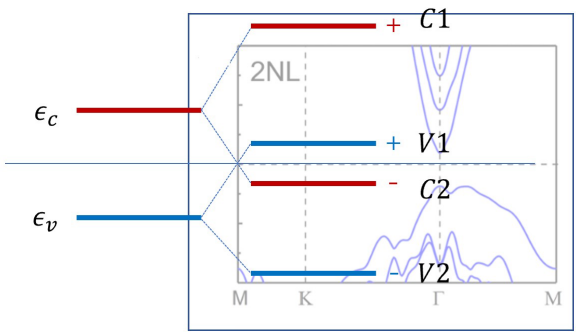

FIG. 9. Band inverse of the 2NL system. The + (−) represents the band parity of even (odd). The bands in the shaded area are the density functional theory (DFT) result [Fig. 6(b)].

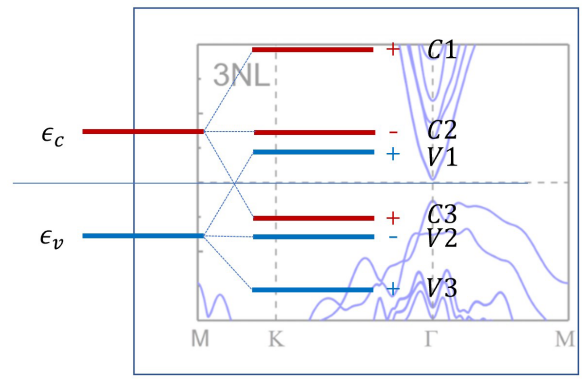

FIG. 10. Band inverse of the 3NL system. The red + (−) represents the band parity of even (odd). The bands in the shaded region are the density functional theory (DFT) result, taken from Fig. 6(c).

TABLE III. Solutions of the 3NL Hamiltonian.

Order	Band energy	Wave function	Parity
C1	$\epsilon_c + \sqrt{2}t_c$	$1, 0, \sqrt{2}, 0, 1, 0$	+
C2	ϵ_c	$-1, 0, 0, 0, 1, 0$	−
C3	$\epsilon_c - \sqrt{2}t_c$	$1, 0, -\sqrt{2}, 0, 1, 0$	+
V1	$\epsilon_v + \sqrt{2}t_v$	$0, 1, 0, \sqrt{2}, 0, 1$	+
V2	ϵ_v	$0, -1, 0, 0, 0, 1$	−
V3	$\epsilon_v - \sqrt{2}t_v$	$0, 1, 0, -\sqrt{2}, 0, 1$	+

(Fig. 10). Compared with simple stacking of three layers of $Z_2 = 0$, the band inversion of C3 and V1 with even parity does not change the topology, and 3NL is in the trivial topological state of $Z_2 = 0$.

For the 4NL system, considering the limitation of the 2NL case, $\epsilon_c - \frac{\sqrt{5}+1}{2}t_c < \epsilon_c - t_c < \epsilon_v + t_v < \epsilon_v + \frac{\sqrt{5}+1}{2}t_v$, we can also have C4 with parity − and V1 with parity + inverted (Table IV). To realize $Z_2 = 1$ for 4NL, C3 and V2 with opposite parities should not invert. Thus, there is an additional limitation $\epsilon_c - \frac{\sqrt{5}-1}{2}t_c > \epsilon_v + \frac{\sqrt{5}-1}{2}t_v$. With a similar analysis for 5NL, we can easily find C4, C5 with parity −, + invert with V1, V2 with parity +, − (Table V). This band inversion does not change the total parity of valence bands compared with the simple stacking system, and 5NL is of $Z_2 = 0$.

The Hamiltonian of 6NL is much more complex and has no analytic solution, so we solve it numerically. Without loss of generality, we assume $\epsilon_c = -\epsilon_v = 1$, $t_c = t_v = \frac{\epsilon_c}{r}$. From the above analysis, r should satisfy $\frac{\sqrt{5}-1}{2} < r < 1$ to reproduce the topological states of 2–5NL cases. However, we find that r should be $0.01 < r < 0.45$ to reproduce the first-principles calculation of the 6NL case. There is no same set of these parameters to reproduce all six cases. The proposed effective mode Hamiltonian might be oversimplified as the thickness increases. Here, 6NL is quite thick and close to the 3D bulk feature. Its band gap is very small (∼5 meV), and it is much closer to the 3D topological phase transition point than the thinner cases. Thus, its topological state is sensitive to details for the first-principles calculation, such as the relaxed interlayer distance and atomic positions in layers. On considering these facts, we believe that this effective model is quite good and has revealed the underlying physical mechanism for the topological phase oscillation with thickness. We realized that there are some other assumptions for parameters in this model Hamiltonian, which have been discussed in the Supplemental Material [55]. The one discussed in this paper is better to be consistent with first-principles results.

TABLE IV. Solutions of the 4NL Hamiltonian.

Order	Band energy	Wave function	Parity
C1	$\epsilon_c + \frac{\sqrt{5}+1}{2}t_c$	$1, 0, \frac{\sqrt{2}+1}{2}, 0, \frac{\sqrt{2}+1}{2}, 0, 1, 0$	+
C2	$\epsilon_c + \frac{\sqrt{5}-1}{2}t_c$	$-1, 0, -\frac{\sqrt{5}-1}{2}, 0, \frac{\sqrt{5}-1}{2}, 0, 1, 0$	−
C3	$\epsilon_c - \frac{\sqrt{5}-1}{2}t_c$	$1, 0, -\frac{\sqrt{5}-1}{2}, 0, -\frac{\sqrt{5}-1}{2}, 0, 1, 0$	+
C4	$\epsilon_c - \frac{\sqrt{5}+1}{2}t_c$	$-1, 0, \frac{\sqrt{2}+1}{2}, 0, -\frac{\sqrt{2}+1}{2}, 0, 1, 0$	−
V1	$\epsilon_v + \frac{\sqrt{5}+1}{2}t_v$	$0, 1, 0, \frac{\sqrt{2}+1}{2}, 0, \frac{\sqrt{2}+1}{2}, 0, 1$	+
V2	$\epsilon_v + \frac{\sqrt{5}-1}{2}t_v$	$0, -1, 0, -\frac{\sqrt{5}-1}{2}, 0, \frac{\sqrt{5}-1}{2}, 0, 1$	−
V3	$\epsilon_v - \frac{\sqrt{5}-1}{2}t_v$	$0, 1, 0, -\frac{\sqrt{5}-1}{2}, 0, -\frac{\sqrt{5}-1}{2}, 0, 1$	+
V4	$\epsilon_v - \frac{\sqrt{5}+1}{2}t_v$	$0, -1, 0, \frac{\sqrt{2}+1}{2}, 0, -\frac{\sqrt{2}+1}{2}, 0, 1$	−

TABLE V. Solutions of the 5NL Hamiltonian.

Order	Band energy	Wave function	Parity
C1	$\epsilon_c + \sqrt{3}t_c$	$1, 0, \sqrt{3}, 0, 2, 0, \sqrt{3}, 0, 1, 0$	+
C2	$\epsilon_c + t_c$	$-1, 0, -1, 0, 0, 0, 1, 0, 1, 0$	−
C3	ϵ_c	$1, 0, 0, 0, -1, 0, 0, 0, 1, 0$	+
C4	$\epsilon_c - t_c$	$-1, 0, 1, 0, 0, 0, -1, 0, 1, 0$	−
C5	$\epsilon_c - \sqrt{3}t_c$	$1, 0, -\sqrt{3}, 0, 2, 0, -\sqrt{3}, 0, 1, 0$	+
V1	$\epsilon_v + \sqrt{3}t_v$	$0, 1, 0, \sqrt{3}, 0, 2, 0, \sqrt{3}, 0, 1$	+
V2	$\epsilon_v + t_v$	$0, -1, 0, -1, 0, 0, 0, 1, 0, 1$	−
V3	ϵ_v	$0, 1, 0, 0, 0, -1, 0, 0, 0, 1$	+
V4	$\epsilon_v - t_v$	$0, -1, 0, 1, 0, 0, 0, -1, 0, 1$	−
V5	$\epsilon_v - \sqrt{3}t_v$	$0, 1, 0, -\sqrt{3}, 0, 2, 0, -\sqrt{3}, 0, 1$	+

IV. CONCLUSIONS

In this paper, we investigate the topological properties with respect to the stacking orders and film thicknesses of the layered $M_2Bi_2Te_5$ (M = Ge, Sn, Pb) materials. We find that monolayer $M_2Bi_2Te_5$'s are all indirect band-gap semiconductors, and the multilayer structures are all direct band-gap semiconductors. The bilayer $M_2Bi_2Te_5$ (M = Ge, Sn, Pb) films with the most stable stacking orders of *ABC-ABC* are all TIs because of the effective parity inversion. Due to the strong SOC, bilayer $Pb_2Bi_2Te_5$ has a band gap of 111.6 meV, which is large enough to observe the QSH effect and stacking-order-related properties in experiments at room temperature in the systems. The 2NL-3/2NL-1 $Pb_2Bi_2Te_5$ films can become topologically nontrivial/trivial insulators by shortening/enlarging the interlayer distance. Very interestingly, $Pb_2Bi_2Te_5$ films are found to have unique topological phase oscillation effects as the film thickness increases, rationalized by the proposed nearest-neighbor interlayer coupling model. In this paper, we provide an excellent material platform for the experimental realization and tuning of the QSH effect.

ACKNOWLEDGMENTS

This paper was supported by the National Natural Science Foundation of China (Grants No. 12174059, No. 11874117, No. 11604134, No. 11925408, No. 11921004, and No. 12188101), the Ministry of Science and Technology of China (Grants No. 2018YFA0305700 and No. 2022YFA1403800), the Chinese Academy of Sciences (Grant No. XDB33000000), the Informatization Plan of Chinese Academy of Sciences (Grant No. CAS-WX2021SF-0102), and the Natural Science Foundation of Shanghai (Grant No. 21ZR140820). The calculations were performed at the High Performance Computational Center of the Department of Physics at Fudan University.

Y.L. and Y.J. contributed equally to this paper.

[1] C. L. Kane and E. J. Mele, Phys. Rev. Lett. **95**, 146802 (2005).
[2] C. L. Kane and E. J. Mele, Phys. Rev. Lett. **95**, 226801 (2005).
[3] B. A. Bernevig, T. L. Hughes, and S.-C. Zhang, Science **314**, 1757 (2006).
[4] M. Koenig, S. Wiedmann, C. Bruene, A. Roth, H. Buhmann, L. W. Molenkamp, X.-L. Qi, and S.-C. Zhang, Science **318**, 766 (2007).
[5] L. Fu, C. L. Kane, and E. J. Mele, Phys. Rev. Lett. **98**, 106803 (2007).
[6] M. Z. Hasan and C. L. Kane, Rev. Mod. Phys. **82**, 3045 (2010).
[7] X.-L. Qi and S.-C. Zhang, Rev. Mod. Phys. **83**, 1057 (2011).
[8] Y. Tokura, K. Yasuda, and A. Tsukazaki, Nat. Rev. Phys. **1**, 126 (2019).
[9] J. Wang and S.-C. Zhang, Nat. Mater. **16**, 1062 (2017).
[10] Y. Cao, V. Fatemi, S. Fang, K. Watanabe, T. Taniguchi, E. Kaxiras, and P. Jarillo-Herrero, Nature (London) **556**, 43 (2018).
[11] Y. Cao, V. Fatemi, A. Demir, S. Fang, S. L. Tomarken, J. Y. Luo, J. D. Sanchez-Yamagishi, K. Watanabe, T. Taniguchi, E. Kaxiras *et al.*, Nature (London) **556**, 80 (2018).
[12] T. Ohta, J. T. Robinson, P. J. Feibelman, A. Bostwick, E. Rotenberg, and T. E. Beechem, Phys. Rev. Lett. **109**, 186807 (2012).
[13] H. Schmidt, T. Luedtke, P. Barthold, E. McCann, V. I. Fal'ko, and R. J. Haug, Appl. Phys. Lett. **93**, 172108 (2008).
[14] M. Yankowitz, S. Chen, H. Polshyn, Y. Zhang, K. Watanabe, T. Taniguchi, D. Graf, A. F. Young, and C. R. Dean, Science **363**, 1059 (2019).
[15] M. Serlin, C. L. Tschirhart, H. Polshyn, Y. Zhang, J. Zhu, K. Watanabe, T. Taniguchi, L. Balents, and A. F. Young, Science **367**, 900 (2020).
[16] L. Xian, D. M. Kennes, N. Tancogne-Dejean, M. Altarelli, and A. Rubio, Nano Lett. **19**, 4934 (2019).
[17] K. F. Mak, M. Y. Sfeir, J. A. Misewich, and T. F. Heinz, Proc. Natl. Acad. Sci. USA **107**, 14999 (2010).
[18] S. Tongay, J. Zhou, C. Ataca, K. Lo, T. S. Matthews, J. Li, J. C. Grossman, and J. Wu, Nano Lett. **12**, 5576 (2012).
[19] X. Luo, Y. Zhao, J. Zhang, Q. Xiong, and S. Y. Quek, Phys. Rev. B **88**, 075320 (2013).
[20] Y. Zhao, J. Qiao, P. Yu, Z. Hu, Z. Lin, S. P. Lau, Z. Liu, W. Ji, and Y. Chai, Adv. Mater. **28**, 2399 (2016).
[21] P. Jiang, C. Wang, D. Chen, Z. Zhong, Z. Yuan, Z.-Y. Lu, and W. Ji, Phys. Rev. B **99**, 144401 (2019).
[22] S. Woo, H. C. Park, and Y.-W. Son, Phys. Rev. B **93**, 075420 (2016).
[23] P. Zereshki, Y. Wei, R. Long, and H. Zhao, J. Phys. Chem. Lett. **9**, 5970 (2018).
[24] B. Lian, Z. Liu, Y. Zhang, and J. Wang, Phys. Rev. Lett. **124**, 126402 (2020).
[25] C.-X. Liu, H. Zhang, B. Yan, X.-L. Qi, T. Frauenheim, X. Dai, Z. Fang, and S.-C. Zhang, Phys. Rev. B **81**, 041307 (2010).
[26] B. Singh, H. Lin, R. Prasad, and A. Bansil, Phys. Rev. B **88**, 195147 (2013).
[27] I. V. Silkin, Y. M. Koroteev, S. V. Eremeev, G. Bihlmayer, and E. V. Chulkov, JETP Lett. **94**, 217 (2011).
[28] Q. Tong, H. Yu, Q. Zhu, Y. Wang, X. Xu, and W. Yao, Nat. Phys. **13**, 356 (2017).
[29] I. Tateishi and M. Hirayama, Phys. Rev. Res. **4**, 043045 (2022).
[30] J. Li, Y. Li, S. Du, Z. Wang, B.-L. Gu, S.-C. Zhang, K. He, W. Duan, and Y. Xu, Sci. Adv. **5**, eaaw5685 (2019).
[31] D. Zhang, M. Shi, T. Zhu, D. Xing, H. Zhang, and J. Wang, Phys. Rev. Lett. **122**, 206401 (2019).
[32] Y. Gong, J. Guo, J. Li, K. Zhu, M. Liao, X. Liu, Q. Zhang, L. Gu, L. Tang, X. Feng *et al.*, Chin. Phys. Lett. **36**, 089901 (2019).
[33] M. M. Otrokov, I. I. Klimovskikh, H. Bentmann, D. Estyunin, A. Zeugner, Z. S. Aliev, S. Gaß, A. U. B. Wolter, A. V.Koroleva, A. M. Shikin *et al.*, Nature (London) **576**, 416 (2019).
[34] Y. Deng, Y. Yu, M. Z. Shi, Z. Guo, Z. Xu, J. Wang, X. H. Chen, and Y. Zhang, Science **367**, 895 (2020).
[35] C. Liu, Y. Wang, H. Li, Y. Wu, Y. Li, J. Li, K. He, Y. Xu, J. Zhang, and Y. Wang, Nat. Mater. **19**, 522 (2020).
[36] J. Ge, Y. Liu, J. Li, H. Li, T. Luo, Y. Wu, Y. Xu, and J. Wang, Natl. Sci. Rev. **7**, 1280 (2020).
[37] Y. Li, Y. Jiang, J. Zhang, Z. Liu, Z. Yang, and J. Wang, Phys. Rev. B **102**, 121107 (2020).
[38] J. Zhang, D. Wang, M. Shi, T. Zhu, H. Zhang, and J. Wang, Chin. Phys. Lett. **37**, 077304 (2020).
[39] L. Cao, S. Han, Y.-Y. Lv, D. Wang, Y.-C. Luo, Y.-Y. Zhang, S.-H. Yao, J. Zhou, Y. B. Chen, H. Zhang *et al.*, Phys. Rev. B **104**, 054421 (2021).
[40] R. Peng, Y. Ma, H. Wang, B. Huang, and Y. Dai, Phys. Rev. B **101**, 115427 (2020).
[41] A. Chatterjee and K. Biswas, Angew. Chem. Int. Ed. **54**, 5623 (2015).
[42] T. Matsunaga, R. Kojima, N. Yamada, K. Kifune, Y. Kubota, and M. Takata, Acta. Cryst. B **63**, 346 (2007).
[43] B. A. Kuropatwa and H. Kleinke, Z. Anorg. Allg. Chem. **638**, 2640 (2012).
[44] C.-N. Chiu, C.-M. Hsu, S.-W. Chen, and H.-J. Wu, J. Electron. Mater. **41**, 22 (2012).
[45] P. E. Blöchl, Phys. Rev. B **50**, 17953 (1994).
[46] G. Kresse and J. Furthmüller, Phys. Rev. B **54**, 11169 (1996).
[47] J. P. Perdew, K. Burke, and M. Ernzerhof, Phys. Rev. Lett. **77**, 3865 (1996).
[48] S. Grimme, J. Antony, S. Ehrlich, and H. Krieg, J. Chem. Phys. **132**, 154104 (2010).
[49] N. Marzari and D. Vanderbilt, Phys. Rev. B **56**, 12847 (1997).
[50] I. Souza, N. Marzari, and D. Vanderbilt, Phys. Rev. B **65**, 035109 (2001).
[51] A. A. Mostofi, J. R. Yates, Y.-S. Lee, I. Souza, D. Vanderbilt, and N. Marzari, Comput. Phys. Commun. **178**, 685 (2008).
[52] Q. Wu, S. Zhang, H.-F. Song, M. Troyer, and A. A. Soluyanov, Comput. Phys. Commun. **224**, 405 (2018).
[53] A. Togo and I. Tanaka, Scr. Mater. **108**, 1 (2015).
[54] A. Togo, F. Oba, and I. Tanaka, Phys. Rev. B **78**, 134106 (2008).
[55] See Supplemental Material at http://link.aps.org/supplemental/10.1103/PhysRevB.108.085428 for some detailed results of bilayer $M_2Bi_2Te_5$ (M = Ge, Sn, Pb) films, the band structures of 1NL $Ge_2Bi_2Te_5$ and 2NL $Pb_2Bi_2Te_5$ with the different stacking orders, the band gaps of bilayer $Pb_2Bi_2Te_5$ under strain, and some extended discussion on the model Hamiltonian.
[56] R. Zacharia, H. Ulbricht, and T. Hertel, Phys. Rev. B **69**, 155406 (2004).
[57] S. Wu, V. Fatemi, Q. D. Gibson, K. Watanabe, T. Taniguchi, R. J. Cava, and P. Jarillo-Herrero, Science **359**, 76 (2018).